SLOAN DIGITAL SKY SURVEY IMAGING OF LOW GALACTIC LATITUDE FIELDS: TECHNICAL SUMMARY AND DATA RELEASE

DOUGLAS P. FINKBEINER,[1,2] NIKHIL PADMANABHAN,[3] DAVID J. SCHLEGEL,[2] MICHAEL A. CARR,[2] JAMES E. GUNN,[2]
CONSTANCE M. ROCKOSI,[1,4] MAKI SEKIGUCHI,[5] ROBERT H. LUPTON,[2] G. R. KNAPP,[2] ŽELJKO IVEZIĆ,[2] MICHAEL R. BLANTON,[6]
DAVID W. HOGG,[6] JENNIFER K. ADELMAN-MCCARTHY,[7] JAMES ANNIS,[7] JEFFREY HAYES,[8] ELLYNNE KINNEY,[9] DANIEL C. LONG,[9]
UROŠ SELJAK,[3] MICHAEL A. STRAUSS,[2] BRIAN YANNY,[7] MARCEL A. AGÜEROS,[4] SAHAR S. ALLAM,[10] SCOTT F. ANDERSON,[4]
NETA A. BAHCALL,[2] IVAN K. BALDRY,[11] MARIANGELA BERNARDI,[12] WILLIAM N. BOROSKI,[7] JOHN W. BRIGGS,[13] J. BRINKMANN,[9]
ROBERT J. BRUNNER,[14] TAMÁS BUDAVÁRI,[11] FRANCISCO J. CASTANDER,[15] KEVIN R. COVEY,[4] ISTVÁN CSABAI,[11,16] MAMORU DOI,[17]
FENG DONG,[2] DANIEL J. EISENSTEIN,[18] XIAOHUI FAN,[18] SCOTT D. FRIEDMAN,[19] MASATAKA FUKUGITA,[20] BRUCE GILLESPIE,[9]
EVA K. GREBEL,[21] VIJAY K. GURBANI,[7,22] ERNST DE HAAS,[2] FREDERICK H. HARRIS,[23] JOHN S. HENDRY,[7] GREGORY S. HENNESSY,[24]
SEBASTIAN JESTER,[7] DAVID E. JOHNSTON,[2] ANDERS M. JORGENSEN,[25] MARIO JURIĆ,[2] STEPHEN M. KENT,[7] ALEXEI YU. KNIAZEV,[21]
JUREK KRZESIŃSKI,[9,26] R. FRENCH LEGER,[7] HUAN LIN,[7] JON LOVEDAY,[27] ED MANNERY,[4] DAVID MARTÍNEZ-DELGADO,[21]
PEREGRINE M. MCGEHEE,[10,28] AVERY MEIKSIN,[29] JEFFREY A. MUNN,[23] ERIC H. NEILSEN, JR.,[7] PETER R. NEWMAN,[9]
ATSUKO NITTA,[9] GEORGE PAULS,[2] THOMAS R. QUINN,[4] R. R. RAFIKOV,[30] GORDON T. RICHARDS,[2] MICHAEL W. RICHMOND,[31]
DONALD P. SCHNEIDER,[32] JOSHUA SCHROEDER,[2] KAZU SHIMASAKU,[33] WALTER A. SIEGMUND,[34] J. ALLYN SMITH,[25,35]
STEPHANIE A. SNEDDEN,[9] ALBERT STEBBINS,[7] ALEXANDER S. SZALAY,[11] GYULA P. SZOKOLY,[36] MAX TEGMARK,[37]
DOUGLAS L. TUCKER,[7] ALAN UOMOTO,[11,38] DANIEL E. VANDEN BERK,[39] DAVID H. WEINBERG,[40]
ANDREW A. WEST,[4] NAOKI YASUDA,[20] D. R. YOCUM,[7] DONALD G. YORK,[41,42] AND IDIT ZEHAVI[18]

ABSTRACT

The Sloan Digital Sky Survey (SDSS) mosaic camera and telescope have obtained five-band optical-wavelength imaging near the Galactic plane outside of the nominal survey boundaries. These additional data were obtained during commissioning and subsequent testing of the SDSS observing system, and they provide unique wide-area imaging data in regions of high obscuration and star formation, including numerous young stellar objects, Herbig-Haro objects, and young star clusters. Because these data are outside the survey regions in the Galactic caps, they are not part of the standard SDSS data releases. This paper presents imaging data for 832 square degrees of sky (including repeats), in the star-forming regions of Orion, Taurus, and Cygnus. About 470 deg^2 are now released to the public, with the remainder to follow at the time of SDSS Data Release 4. The public data in Orion include the star-forming region NGC 2068/NGC 2071/HH 24 and a large part of Barnard's loop.

Key words: atlases — catalogs — surveys

1. INTRODUCTION

The Sloan Digital Sky Survey (SDSS) is a five-band photometric survey of 8500 square degrees of the northern sky and a concurrent redshift survey of nearly a million galaxies and 100,000 quasars selected from the imaging survey (York et al. 2000). The primary purpose of the project is to investigate the large-scale structure of the universe and pursue other extragalactic science. The official survey region therefore largely lies above Galactic latitude $|b| > 30°$ and was carefully chosen to minimize the effect of the troublesome dust near the Galactic plane. This naturally excludes some of the most beautiful parts of the sky, and those areas of most interest for Galactic science.

However, a significant amount of imaging data *has* been obtained at low Galactic latitude by SDSS, both during telescope commissioning and for calibration at sidereal times when the main survey region was unavailable. During commissioning, the SDSS camera (Gunn et al. 1998) was operational before the telescope control system was stable. The camera data acquisition is carried out in drift-scan, or "time-delay and integrate" (TDI), mode, with the camera crossing the sky at the sidereal rate; the large field of view (3°) mandates that this be done along great circles. Accordingly, much of the commissioning work was done by parking the telescope at the celestial equator and drift-scanning the sky. During commissioning observations in the fall of 1998 (when the south Galactic polar cap was available for observation), the drift-scanning continued outside the SDSS survey area and passed through NGC 2068 and NGC 2071 in Orion. Many of the commissioning runs produced data of high scientific quality, some of which are part of the SDSS Early Data Release (EDR; Stoughton et al. 2002), where a detailed description of the imaging data can be found. SDSS runs 259 and 273 generated targets for spectroscopic commissioning, resulting in the first extremely metal-poor galaxy found by SDSS (Kniazev et al. 2003), but have never been made public. Since 1999, additional imaging data at low Galactic latitudes have been obtained for a variety of testing and calibration purposes. However, none of these low-latitude data, external to the SDSS survey area, are included in the SDSS data releases (to date, the EDR, the first data release, DR1 [Abazajian et al. 2003], and DR2 [Abazajian et al. 2004]). We have reduced and calibrated these data as part of a rereduction and recalibration of all the imaging data (the "übercalibration"; Schlegel et al. 2004), and we describe these data in the present paper.

The areas of sky observed are described in § 2. The data products described herein are very similar to those distributed in the previous SDSS data releases but differ in photometric calibration and data format. These differences are described in § 3, and some examples of science applications are briefly discussed in § 4. The data from 1998–1999 are publicly released with this paper and may be accessed via the World Wide Web.[43]

2. THE DATA

2.1. *Sky Coverage*

The sky coverage of the imaging runs to date outside the SDSS area is given in Table 1 and Figure 1. The figure shows the footprint of the survey (including these runs) in equatorial coordinates and indicates the approximate locations of the images in Figures 2, 3, and 4. Table 1 provides information about the location and image quality of each run. An imaging run consists of six long images in each filter, each the width of one CCD (13′52 on the sky) and separated by slightly less than one CCD width (11′65), produced by the six columns of CCDs in the mosaic camera. A run may last the entire night and be over 100° long, or it can be shorter. A *strip* is the area covered by the six camera columns from one survey pole to the other; a *stripe* is a pair of interleaving *strips* and completely covers a 2°5 × 180° stripe on the sky. The imaging data are divided into 8′98 × 13′52 *frames* for further processing; the aligned frames in the five bands are called a *field*. Since the sky passes through the *u*, *g*, *r*, *i*, and *z* SDSS filters in succession (in order *riuzg*), there is a ramp-up time corresponding to 10 frames at the start of each imaging run. Focus and tracking adjustments are made at the beginning of each run, adding variable amounts of overhead to the ramp-up time. The range of fields for each run given in Table 1 defines the range of useful data. A detailed description of the observing procedures is given by Gunn et al. (1998) and York et al. (2000).

The imaging runs comprising the "Orion" data set, released in the present paper, were made in the fall of 1998 and fall of 1999. As Table 1 and Figure 1 show, there have been quite a few low-latitude observations since then, usually for system checking and calibration. Nonphotometric data are included, because proper-motion studies can make use of the astrometry even in unphotometric runs. The data listed in Table 1 are those which, after reduction and processing, prove to be of science quality, and the photometric reliability is indicated.

2.2. *Processing*

The SDSS photometric pipeline consists of four sequential steps: ssc and psp (point-spread function estimation), astrom (Pier et al. 2003; astrometry), and frames (object identification, deblending, and photometry; Lupton et al. 2001; Stoughton et al. 2002; Lupton et al. 2002, 2004). These pipelines run with little human intervention. The photometric pipeline corrects the imaging data by interpolating over defects such as bad columns and cosmic rays; provides flat-field, photometric, and astrometric calibration; and identifies, deblends, measures, and classifies objects. The resulting outputs consist of corrected frames, atlas image cutouts for every object, and a catalog of object positions, magnitudes, and image classifications in the five SDSS bands. The catalog outputs also include flags that describe the image processing, including whether the object contains any saturated pixels, whether bad data were interpolated over, and whether the object was deblended. Careful attention to these processing flags is critical

[33] Department of Astronomy and Research Center for the Early Universe, School of Science, University of Tokyo, 7-3-1 Hongo, Bunkyo, Tokyo 113-0033, Japan.

[34] Institute for Astronomy, University of Hawaii, 2680 Woodlawn Drive, Honolulu, HI 96822.

[35] Department of Physics and Astronomy, University of Wyoming, P.O. Box 3905, Laramie, WY 82071.

[36] Max-Planck-Institut für extraterrestrische Physik, Giessenbachstrasse 1, D-85741 Garching, Germany.

[37] Department of Physics and Astronomy, University of Pennsylvania, 209 South 33rd Street, Philadelphia, PA 19104.

[38] Carnegie Observatories, 813 Santa Barbara Street, Pasadena, CA 91101.

[39] Department of Physics and Astronomy, University of Pittsburgh, 3941 O'Hara Street, Pittsburgh, PA 15260.

[40] Department of Astronomy, Ohio State University, 140 West 18th Avenue, Columbus, OH 43210.

[41] Department of Astronomy and Astrophysics, University of Chicago, 5640 South Ellis Avenue, Chicago, IL 60637.

[42] Enrico Fermi Institute, University of Chicago, 5640 South Ellis Avenue, Chicago, IL 60637.

[43] At http://photo.astro.princeton.edu (hereafter "the Web site"). Future data releases will also be accessible at this site.

TABLE 1
SDSS GALACTIC PLANE RUNS

Run (1)	UT Date (2)	MJD (3)	Strip (4)	Node (deg) (5)	Incl. (deg) (6)	F_0 (7)	F_1 (8)	A (deg^2) (9)	l (deg) (10)	b (deg) (11)	PSF (arcsec) (12)	Phot.? (13)
211..............	1998 Oct 29	51,115	82S	283.22	0.01	11	385	71.2	210.2	−3.3	1.36	Y
250..............	1998 Nov 16	51,133	82N	62.10	0.02	11	455	84.5	201.9	−18.0	1.55	Y
259..............	1998 Nov 17	51,134	82N	299.41	0.01	12	567	105.6	206.7	−9.5	1.19	Y
273..............	1998 Nov 19	51,136	82S	286.54	0.01	11	534	99.6	206.1	−11.1	1.41	N
297..............	1998 Nov 22	51,139	82O	92.04	0.04	11	203	36.7	206.0	−11.0	1.47	Y
307..............	1998 Nov 23	51,140	82N	318.93	0.01	11	186	33.4	212.4	0.0	1.21	N
308..............	1998 Nov 23	51,140	10N	271.30	0.01	11	216	39.1	216.0	4.2	1.24	Y
994..............	1999 Oct 6	51,457	76S	275.04	15.00	11	133	23.4	209.9	−5.0	1.84	N
1923.............	2000 Dec 8	51,886	0O	215.00	44.99	29	71	8.2	86.4	0.0	1.75	U
1924.............	2000 Dec 8	51,886	0O	354.00	45.99	34	78	8.6	168.6	11.9	1.88	U
1925.............	2000 Dec 8	51,886	0O	349.98	45.78	17	48	6.1	165.3	6.6	1.60	U
2955.............	2002 Feb 7	52,312	82N	9.82	0.00	21	166	27.7	209.3	−4.5	2.07	Y
2960.............	2002 Feb 8	52,313	82S	25.79	0.01	11	127	22.2	208.0	−7.4	1.16	Y
2968.............	2002 Feb 9	52,314	82N	90.64	0.00	19	94	14.4	207.8	−7.3	1.68	Y
3511.............	2002 Dec 6	52,614	0O	65.19	90.14	14	89	14.4	163.5	−8.2	1.17	Y
3512.............	2002 Dec 6	52,614	0O	335.41	25.32	11	90	15.2	177.3	−9.3	1.22	Y
3557.............	2002 Dec 31	52,639	0O	65.50	89.96	11	87	14.6	165.6	−10.5	1.26	Y
3559.............	2002 Dec 31	52,639	0O	335.41	25.31	11	86	14.4	176.4	−9.9	1.20	Y
3610.............	2003 Jan 27	52,666	61N	274.99	52.50	17	148	25.1	139.0	−10.8	1.63	Y
3628.............	2003 Jan 28	52,667	61S	275.01	52.52	17	165	28.3	137.3	−10.9	0.97	Y
3629.............	2003 Jan 28	52,667	61N	275.00	52.50	11	129	22.6	142.0	−10.9	0.97	Y
3634.............	2003 Jan 29	52,668	62N	275.00	50.01	18	162	27.5	159.1	−13.0	1.04	Y
3642.............	2003 Feb 1	52,671	62S	274.99	49.99	11	97	16.5	135.6	−13.2	1.73	Y
3643.............	2003 Feb 1	52,671	62S	274.99	50.00	11	119	20.7	159.1	−13.2	1.68	Y
4114.............	2003 Sep 20	52,902	0S	309.49	90.02	41	127	16.5	80.1	0.0	1.59	Y
4115.............	2003 Sep 20	52,902	0S	309.34	90.15	11	69	11.2	78.7	0.0	1.36	Y
4116.............	2003 Sep 20	52,902	0O	219.49	41.40	11	77	12.7	82.1	0.0	1.40	Y
4119.............	2003 Sep 20	52,902	0O	309.40	90.08	11	70	11.4	79.8	0.0	1.71	Y

NOTES.—Col. (1): SDSS run number. Col. (2): UT Date. Col. (3): UT MJD. Col. (4): Survey strip number; 82 and 10 are on the celestial equator. N = north, S = south, O = other (non–survey strips). Cols. (5, 6): J2000 node and inclination of stripe great circle. Col. (7): Start field for run; in some cases ramp-up takes more than 11 fields. Col. (8): End field. Col. (9): Gross area in square degrees. Cols. (10, 11): Galactic coordinates of closest approach to the Galactic plane of any field center. Col. (12): Median PSF FWHM (*r*-band, camera column 3). Col. (13): Photometric? (Y = yes, N = no, U = unknown). Run 273 has an aperture obstruction early in the run, and run 307 is slightly cloudy near the end. Data in the 1998–1999 runs are now public.

for proper scientific use of the data. A complete description of the data outputs can be obtained at the Web site mentioned above, at the SDSS DR2 Web site,[44] and in papers by Stoughton et al. (2002) and Abazajian et al. (2003, 2004).

―――――――――

[44] See http://www.sdss.org.

The `frames` pipeline produces a catalog of objects (`fpObjc` files) described by instrumental quantities: (*x*, *y*)-positions on a frame, CCD counts, and radii. Astrometric calibrations are applied by the astrometric pipeline (`astrom`) and are accurate to better than 0″.1 rms in each coordinate (Pier et al. 2003). Because early commissioning data sometimes had poor telescope

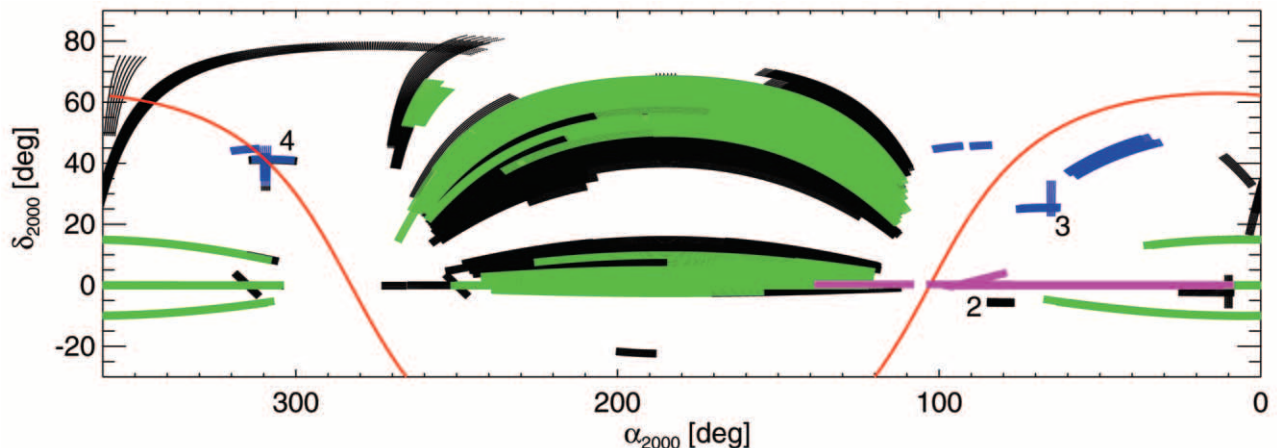
FIG. 1.—The SDSS footprint in equatorial coordinates, consisting of the (currently released) Orion data (*magenta*), other Galactic plane runs (*blue*), SDSS DR2 (*green*), and other SDSS data taken through 2003 December (*black*). Numbers mark the regions shown in Figs. 2–4.
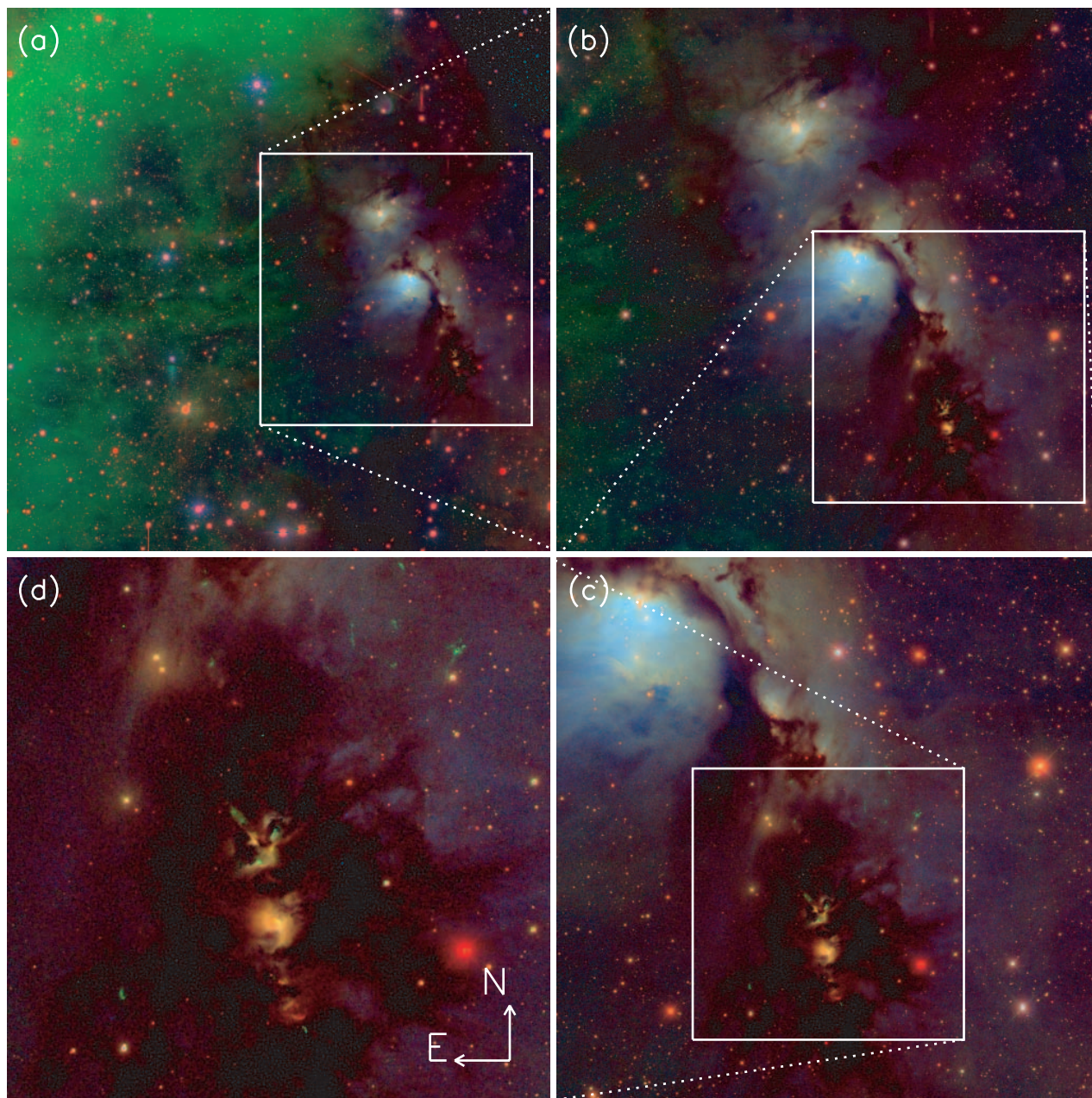
Fig. 2.—Orion: A section of runs 259 and 273 centered at J2000 $(\alpha, \delta) = (05^h48^m28^s, +00°04'48'')$. The red, green, and blue color planes represent the SDSS i, r, and g filters, respectively, so that Hα emission appears green. Celestial north is indicated in (d). The widths of (a–d) are 108′, 54′, 27′, and 13′.5, respectively. The nebulae NGC 2071 (*upper*) and NGC 2068 are visible in (b), and (d) zooms in on the object HH 24 (*upper middle*).

pointing information (pointing errors of up to 0°.5), astrometric preprocessing using the discrete cross-correlation method described by Hogg et al. (2001) has been performed to allow such data to be processed in an automated fashion. The flat-fielding and photometric calibration were derived from a global recalibration using all the available repeat imaging (Schlegel et al. 2004). The zero points of the photometric solutions are forced to agree on average with the calibrations derived from the Photometric Telescope (Fukugita et al. 1996; York et al. 2000; Smith et al. 2002) used in SDSS DR2.

2.2.1. *Automation with* photoop

The importance of a completely automated data processing pipeline cannot be overemphasized; it ensures that all the reductions are carried out in a homogeneous fashion and protects against human biases. Furthermore, it ensures that all reductions are perfectly reproducible, allowing comparisons between different reduction attempts. This is a necessary prerequisite for a survey such as SDSS that targets subsamples of galaxies for follow-up observations, because it enables one to measure the completeness of these subsamples even as the underlying software evolves.

While the standard SDSS pipelines perform well within the standard survey region, the radically different characteristics of the data near the Galactic plane require adjustments of various pipeline parameters to process these data. In order to implement these in an automated manner, we have developed a meta-pipeline, photoop, to manage all aspects of processing. In production mode, the only human intervention required is to specify the runs to be processed; after that, photoop sets up
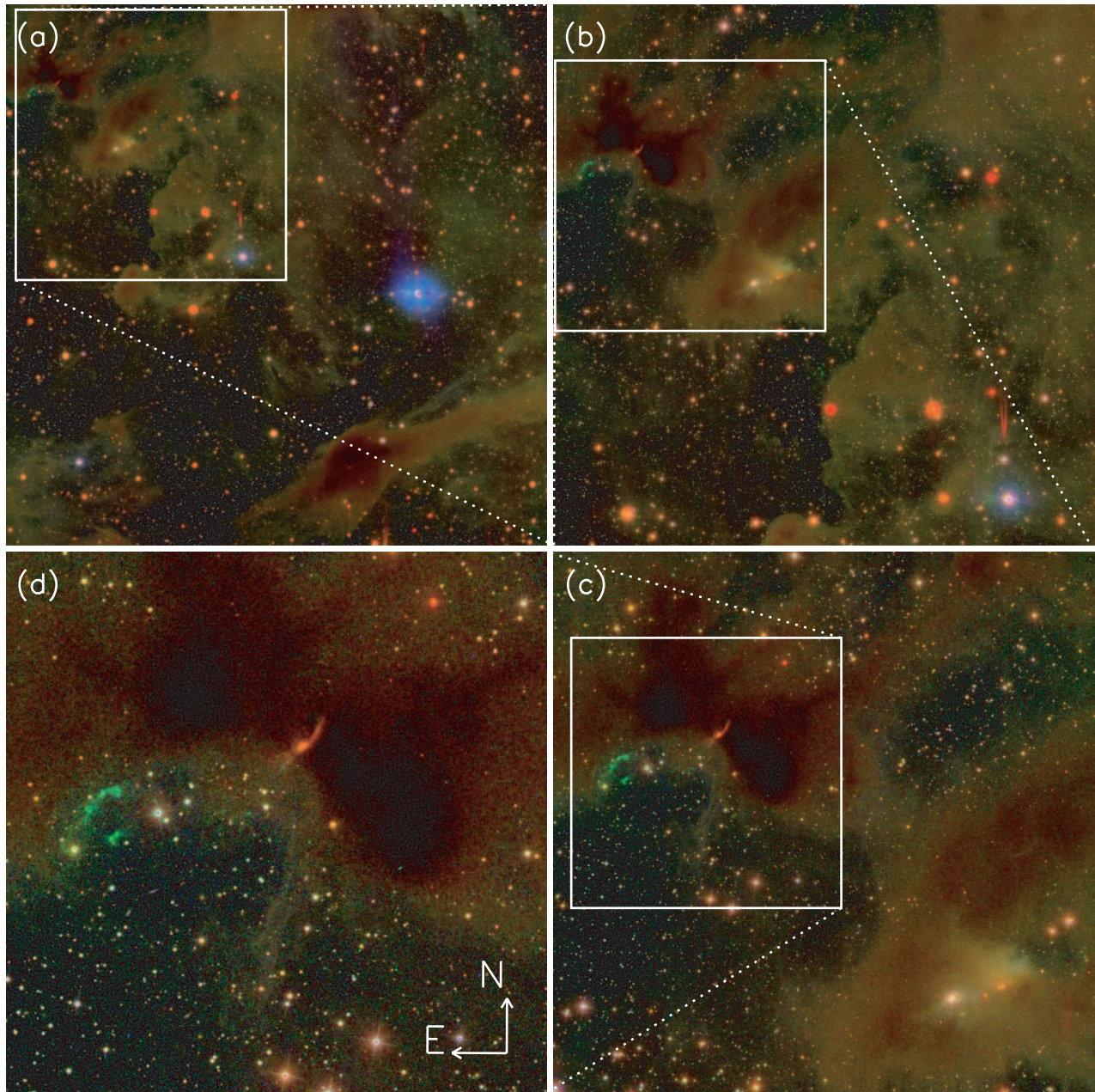
FIG. 3.—Taurus: A section of runs 3512 and 3559 centered at $(\alpha, \delta) = (04^h24^m40^s, +25°41'24'')$. The color scheme and scale are identical to Fig. 2. The large dark cloud in the lower right of (a) is Barnard 215, which joins with Lynds 1506 further to the right; (d) zooms in on HH 31A–31D and associated outflows (*middle left*).

the photometric pipeline and generates the required input data for each run, including flat fields, astrometric catalogs, and configuration files. Perl scripts then manage the actual processing across several Unix servers with a shared network file system. Other photoop scripts automate daily maintenance tasks: monitoring the processing status of each run, posting results to an internal Web page, and testing data integrity. Notices of pipeline failures and data-integrity warnings are automatically sent by E-mail to the responsible parties. Furthermore, photoop has been designed to be portable so that anyone with sufficient computing power and access to the raw data can replicate the entire processing system.

2.2.2. *Processing Software Versions and Reruns*

As the SDSS software pipelines have evolved over time, it has been necessary to keep track of the various processing

attempts with *rerun* numbers. Data processing done by means of photoop is strictly versioned, with rerun numbers above 100 to avoid confusion with the main survey rerun numbers (0−99). There is a one-to-one correspondence between rerun number and software versions. The current rerun as of this writing is 137, corresponding to ssc v5_3_4, astrom v3_7, photo v5_4_25, and v4 flat fields and photoop v1_0. For historical reasons, the psp and frames steps of the pipeline are both part of the photo software product. The instructions below for accessing and using the data refer to rerun 137. Future refinements of the software will have higher rerun numbers and will be announced on the Web site.

2.2.3. *Calibration*

Survey data releases are indirectly calibrated to a set of primary photometric standard stars measured with the US Naval
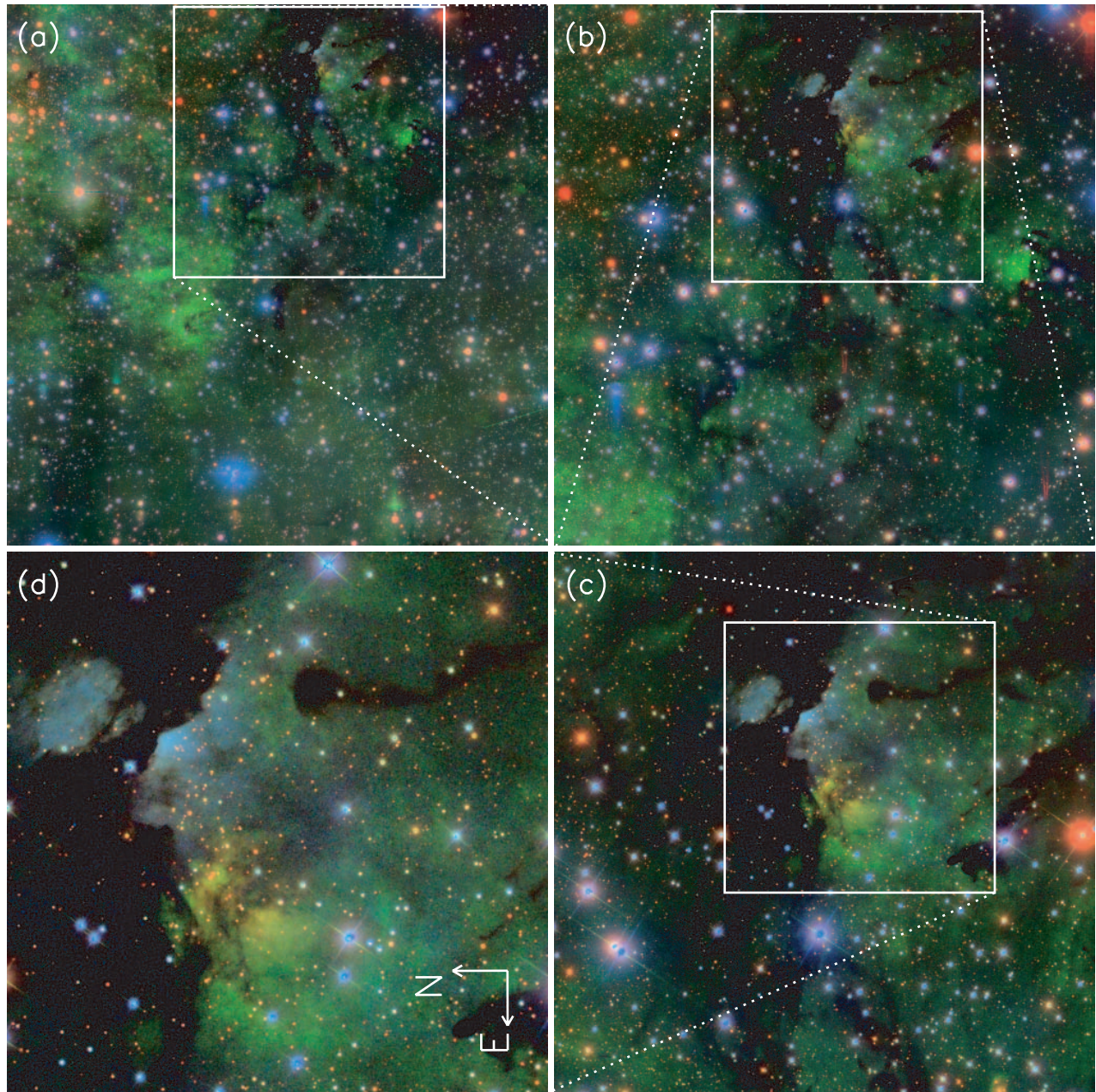
Fig. 4.—Cygnus: A section of runs 4115 and 4119 centered at $(\alpha, \delta) = (20^h36^m04^s, +40°26'24'')$. The color scheme and scale are identical to Fig. 2. The H $_{II}$ region LBN 271 is visible in (a) (*middle left*), and (d) zooms in on a beautiful complex of dark clouds in front of LBN 258.

Observatory (USNO) 1 m telescope in the SDSS filters. This photometric system is denoted by $u'g'r'i'z'$ and is defined by Smith et al. (2002). These primary standards are bright enough to saturate the 2.5 m survey telescope, so the photometric system is transferred to a set of secondary standard star "patches" observed by the 0.5 m "Photometric Telescope" (PT) situated adjacent to the survey telescope. These secondary standards are used to calibrate the 2.5 m native filter system (denoted *ugriz*) to the USNO system for typical star colors. Note that the $u'g'r'i'z'$ and *ugriz* systems are significantly different (see, e.g., Stoughton et al. 2002). PT patches are sparse or nonexistent for much of the Orion region, so we have instead used the übercalibration algorithm (Schlegel et al. 2004) to tie the eight Orion runs together photometrically. This algorithm lets the calibration zero points in each CCD (*a*-terms) and atmospheric extinction (*k*-terms) float night by night, constrained

by multiple observations of stars in run overlaps. Run 308 does not overlap any of the other Orion runs and is therefore calibrated using the same *a*- and *k*-terms as run 307 from the same night. Übercalibration minimizes the rms magnitude residuals in repeat observations of $\sim 10^6$ stars by adjusting these *a*- and *k*-terms. Because the north and south strips of the equatorial stripe overlap only at the camera column edges, and the flat fields are less certain there, it is necessary to use a perpendicular scan (run 2766) to tie the 12 independent camera columns together. This run is connected to the Orion runs by means of four other equatorial runs (94, 125, 1755, 2677). For equatorial drift scans the air mass is constant, making the *a*- and *k*-terms degenerate, so *k*-terms are fixed to canonical values.

Most stars are observed multiple times by this set of runs, and for each star the residual between each run and the mean of all observations of that star is shown in Figure 5. Only stars
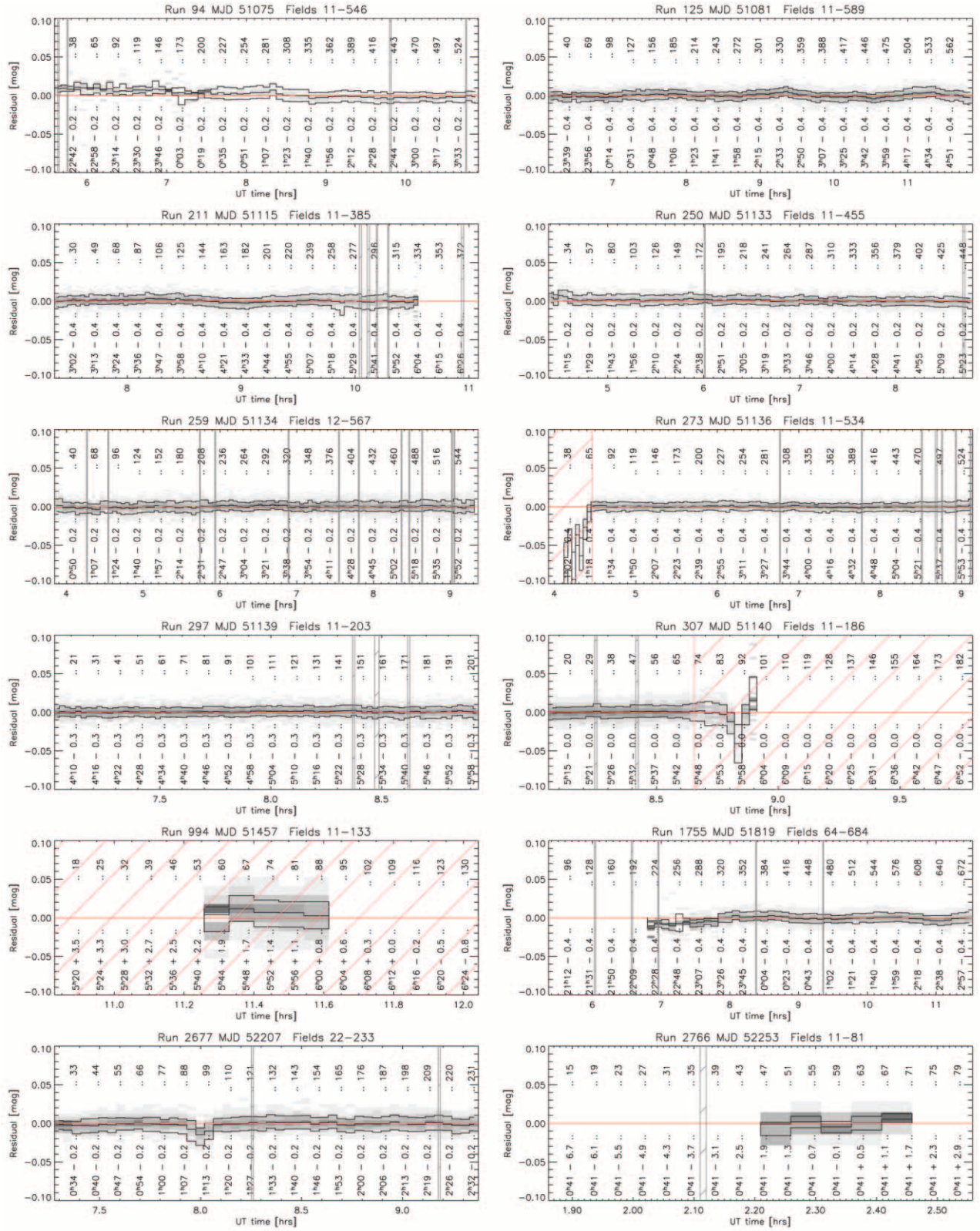
FIG. 5.—Measured magnitudes minus means for each star of each run used in the Orion übercalibration (see § 2.2.3). Stars brighter than 19.0, 19.0, 19.0, 18.5, and 17.0 mag in u, g, r, i, and z respectively are used in the calibration; results are shown for the r band only. Differences are represented as gray scales with 25th, 50th, and 75th percentile lines. Results are similar for g and i bands, with more photometric scatter in u and z (see Fig. 6). Cloudy or otherwise unphotometric data are indicated by red hatches, and gray hatches indicate fields where the pipeline was unable to determine a good point-spread function; these data are not used in fits. Run 308 does not appear here, because it has no overlap with the others, but it is calibrated by fixing its parameters to run 307.
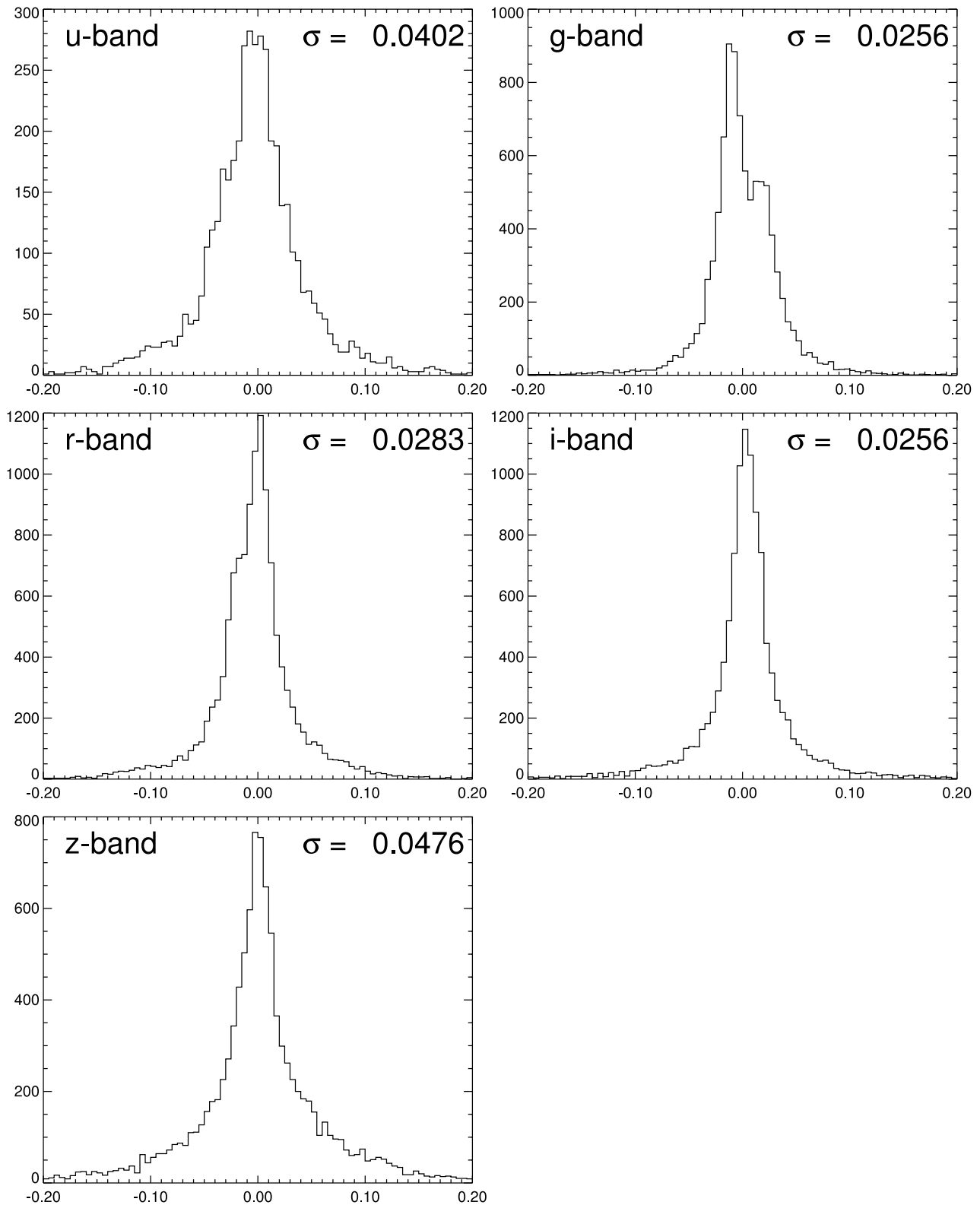
FIG. 6.—Histograms of aperture magnitude differences between runs 259 and 297 for the five SDSS bands. Stars with 7″43 radius aperture magnitudes brighter than 19.0, 19.0, 19.0, 18.5, and 17.0 in u, g, r, i, and z are shown. Note that the measurement uncertainty in each run is a factor of $\sqrt{2}$ smaller than the histogram width. The bimodality in the g band is likely caused by 1%–2% variation in the flat fields with time.

TABLE 2
CVS Products

Product	CVS Version	Language	Analysis?	Description
dust	v0_0	IDL/Fortran/C	Opt.	The Schlegel et al. (1998) $E(B-V)$ extinction maps
eups	v0_4	Perl	Opt.	Product management software
first	v03Apr11	...	Opt.	FIRST (Becker et al. 1995) radio catalog
idlutils	v5_0_0	IDL/Fortran/C	Yes	General IDL tools; *required for all IDL tasks*
photoop....................................	v1_1	Perl/IDL	Yes	SDSS Perl/IDL tools
runList.par...........................	...	...	Yes	The list of runs processed, and their locations
twomass.................................	allsky	...	Opt.	2MASS (Cutri et al. 2003) Point Source Catalog
tycho2....................................	v0_0	...	Opt.	Tycho (Høg et al. 2000) astrometric catalog
ucac	v2_final	...	Opt.	UCAC (Zacharias et al. 2000) astrometric catalog
usno	vB	...	Opt.	USNO-B (Monet et al. 2003) astrometric catalog

Note.—The list of all products used for either processing, analyzing, or accessing the data. We limit ourselves to those products unique to this reduction; the reader is referred to Stoughton et al. (2002) for the official survey pipeline code. The column "Analysis" marks products either necessary ("Yes") or optional ("Opt.") for data analysis.

with $7\rlap{.}''43$ radius aperture magnitudes brighter than 19.0, 19.0, 19.0, 18.5, and 17.0 in u, g, r, i, and z respectively were used for the calibration, and the resulting difference histograms have a 5 σ clipped rms of 40, 26, 28, 26, and 48 mmag (Fig. 6). This calibration method will be described in detail elsewhere (Schlegel et al. 2004), and astrophysical tests of its accuracy will be provided in Finkbeiner et al. (2004).

2.3. *Public Data Access*

Table 2 lists all software and ancillary data products (in addition to the standard survey software described by Stoughton et al. 2002) that are used in the data processing, access, and analysis steps. These products are organized with the Concurrent Versions System (CVS).[45] IDL[46] routines for displaying and calibrating images, extracting photometric parameters for sources, and matching sources to other public catalogs are included. Recipes using some of the most powerful routines are given in examples below. We refer the reader to the Web site for details on downloading and installing these packages; here we limit ourselves to brief descriptions of the data products that make up this data release.

This data release contains three data sets: calibrated images for every field, object catalogs for every field, and trimmed catalogs of "stars" (all point sources, including quasars) and "galaxies" (extended sources) for every run. The images have had cosmic rays removed, had CCD defects corrected, and been flat-fielded and photometrically calibrated. In addition, these images have accurate astrometry stored in a FITS-compliant header and therefore do not depend on any auxiliary information. The object catalogs (calibObj) include all data fields in the uncalibrated fpObjc catalogs produced by the SDSS frames pipeline, as well as calibrated quantities. Object fluxes are calibrated, and the CCD positions of objects are translated to equatorial coordinates using the best-fit astrometric solution from the SDSS astrom pipeline. An overview of the differences between these calibObj catalogs and the standard SDSS tsObj files (available at the Data Archive Server)[47] is given in § 3, and the calibObj format is described in detail in Appendix A.

The calibObj catalogs for the eight public runs require 50 gigabytes. For users who prefer data in a more compact format, we also provide trimmed stellar and galaxy catalogs

for each camera column in each of the eight runs, which total 1.5 Gbyte for the stars and 2.5 Gbyte for the galaxies. The trimmed catalogs contain all stars with any of u, g, r, i, and z brighter than 22.5, 22.5, 22.5, 22.0, and 21.5 mag, respectively, and galaxies brighter than 21.0, 22.0, 22.0, 20.5, and 20.1 mag. These cuts were made after applying the Schlegel et al. (1998, hereafter SFD98) extinction correction for the purpose of object selection—the extinction correction is *not* applied to the flux values in the catalogs. These trimmed star and galaxy catalogs are a strict subset of the quantities described in Appendix A and contain no additional information. The list of fields contained is given on the Web site.

Instructions for downloading any of these data are at the Web site. We advise users to organize downloaded data using the directory structure described there, as this ensures compatibility with our released software.

2.4. *Release Schedule*

Runs 211 through 994, comprising 470 square degrees, are now available to the public at the Web site. Further data will be released on a schedule that approximately parallels that of the SDSS data releases. We plan to release runs through 4119 at the time of SDSS Data Release 4, expected in 2005. Note that these data, unlike the SDSS data releases, contain no spectra.

3. DATA FORMATS

The Galactic plane data processing and data formats differ somewhat from those of SDSS DR2, partly from changes necessary to process these data, and partly to rationalize some naming conventions. The catalogs produced by the current data processing are in calibObj files, whose format we now describe.

1. All data fields output by the frames step of the photometric pipeline in fpObjc files are retained, and not overwritten as they are in tsObj files.

2. Object fluxes are given in linear units, instead of the asinh magnitudes (or "luptitudes"; Lupton et al. 1999) used in the other data releases. This facilitates, for example, co-adding of repeat imaging at the catalog level.

3. Calibrated quantities are presented in nanomaggies (abbreviated nMgy, a flux density), where 1 Mgy is the AB flux density of a zeroth-magnitude flat-spectrum object (Oke & Gunn 1983). An AB magnitude of 22.5 corresponds to 1 nMgy in any filter. The approximate conversion to physical units is

[45] See http://www.cvshome.org.
[46] See http://www.rsinc.com.
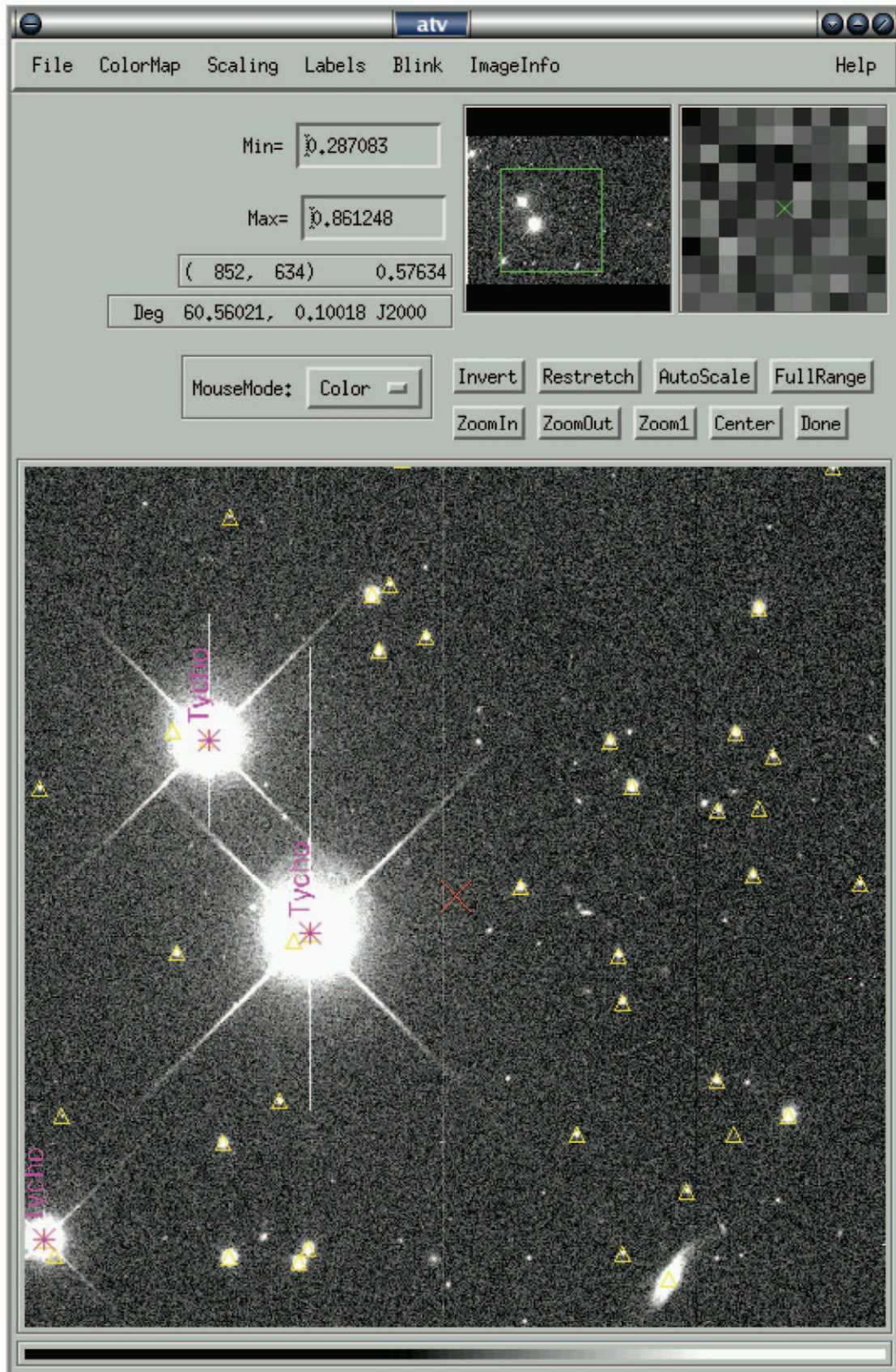[47] See http://das.sdss.org/DR2/data/imaging/; see also Stoughton et al. (2002) for more details.

Fig. 7.—The display tool atvsdss. Here it finds a raw SDSS image at the given coordinates, flat-fields and calibrates on the fly, matches and overplots Tycho stars (*magenta*) and 2MASS stars (*yellow triangles*), and displays a red cross at the requested coordinates. See § 4.1 for more details.

1 Mgy = 3631 Jy, where 1 Jy = 10^{-26} W m^{-2} Hz^{-1} = 10^{-23} ergs s^{-1} cm^{-2} Hz^{-1}. This conversion is only accurate to about 5% (Oke & Gunn 1983), although relative zero-point offsets among the SDSS filters are determined to 1%–2% (Abazajian et al. 2004). Note that the conversion of a measured calibrated magnitude of a source in a broadband filter system to a physical flux density depends on the spectral shape of the source, so precise conversion factors do not exist.

4. Names are rationalized. In fpObjc files, for historical reasons, model counts are known as COUNTS_MODEL and Petrosian counts as PETROCOUNTS. In the standard survey tsObj files these fields are overwritten with calibrated magnitudes, causing confusion. In the calibObj data structure, these uncalibrated data fields appear unchanged, with the corresponding calibrated quantities appended as MODELFLUX and PETROFLUX.

5. Flux uncertainties are nearly Gaussian in the low signal-to-noise limit (unlike errors in magnitudes). We express these errors as an inverse variance ("ivar"). This is convenient for inverse-variance weighting when combining quantities and handles zero signal-to-noise ratio (ivar = 0) gracefully, as demonstrated in Appendix B. Names are, for example, PETROFLUX_IVAR.

6. Extinction in magnitudes (from SFD98) is given in the five SDSS bands and is called EXTINCTION, not REDDENING as in the tsObj files. These values are calculated assuming the standard $R_V = 3.1$ reddening law (Cardelli et al. 1989), which may be inappropriate for some low-latitude regions.

7. Model profile angles such as PHI_ISO_DEG, PHI_DEV_DEG, and PHI_EXP_DEG are expressed as angles in degrees east of north.

8. PSF_FWHM (arcseconds) is given for every object in each band. Because of the telescope optics and seeing, the PSF varies across a frame. The PSF is modeled by a set of eigenfunctions measured by bright stars in the frame, and the interpolated PSF calculated at the position of every object detected by photo. Note that this same information is available through the adaptive moments of the reconstructed PSF.

9. Wherever possible, objects are matched to the FIRST radio catalog (Becker et al. 1995), the 2MASS Point Source Catalog (Cutri et al. 2003), and the USNO-B astrometric survey (Monet et al. 2003).

4. SCIENCE

The science enabled by the wide-area imaging reported here generally lies in the areas of Galactic structure, star formation, and interstellar matter. Several examples are noted here; for the simplest of these, we also provide fragments of IDL code that illustrate the functionality of our publicly available software (Table 2).

4.1. *Displaying an Image*

Using the photoop tools, one can calibrate the raw image data (idR files) at read time and eliminate the need to store a second, calibrated copy of the image data (Fig. 7). Following is a sequence of IDL commands to find (run, camcol, field) for a position on the sky, read in a calibrated image with astrometric information, match objects in the field to the 2MASS catalog, and display the image with matches overplotted in the IDL display tool atv (Barth 2001).

```
; To see which runs cover RA=60.56, dec=0.1
IDL> imlist=sdss_findimage(60.56,0.1,rerun=137, $
     /print)
```

RA	DEC	RUN	RERUN	CAMCOL	FIELD	XPOS	YPOS
60.5600	0.10000	211	137	4	131	978.10	177.24
60.5600	0.10000	273	137	4	338	917.33	1047.2

```
; read the first image
file=sdss_name('idR', imlist[0].run, $
  imlist[0].camcol, imlist[0].field, filter='r')
sdss_readimage, file, image, ivar, /reject_cr, $
  rerun=137, hdr=hdr

; get astrometry and add to header
gsa_approx = sdss_astrom(imlist[0].run, $
  imlist[0].camcol, imlist[0].field, filter='r')
gsssputast, hdr, gsa_approx

; display the image in the atv widget, which
;   allows panning, zooming, color stretches, etc.,
;   and displays WCS coordinates from a FITS
;   header.
atv, image, header=hdr

; Now match 2MASS stars
fobj = tmass_read(60.56, 0.1, 0.2)
astrom_adxy, gsa_approx, fobj.tmass_ra, $
  fobj.tmass_dec, xpix=xpos, ypix=ypos

; and overplot as yellow triangles
atvplot, xpos, ypos, psym=5, symsize=1.5, $
  color='yellow'
```

The above commands demonstrate the power of some of the tools available. The atv wrapper atvsdss does all of the above with the simple command

```
atvsdss, ra=60.56, dec=0.1, /catalog, rerun=137
```

where the rerun number is required for use of the survey astrom astrometric solutions, and /catalog matches and overplots Tycho stars (Fig. 7, *magenta*), 2MASS stars (*yellow triangles*), and a cross at the requested coordinates (*red*).

4.2. *The Stellar g-r-i Color Diagram*

The following is a simple example that plots the stellar locus in the *g-r-i* color plane and provides an introduction to using the catalog data. We start by reading in all the objects from a segment of a run and then select only the stars with reliable photometry using the object flags. We then demonstrate the conversion of calibrated fluxes into magnitudes and use these to construct a magnitude-limited sample of stars. Finally, we compute and plot the *g−r* and *r−i* colors of these stars. The output of this code is shown in Figure 8.

```
; Open a plot
dfpsplot, 'gricolor.ps', /square, /color

; Read in run 273, camcol 3, fields 50-250
; This reads in the data from the "datasweep"
;   trimmed catalogs
objs = sweep_readobj(273, 3, rerun=137, $
  fieldrange=[50,250])
```
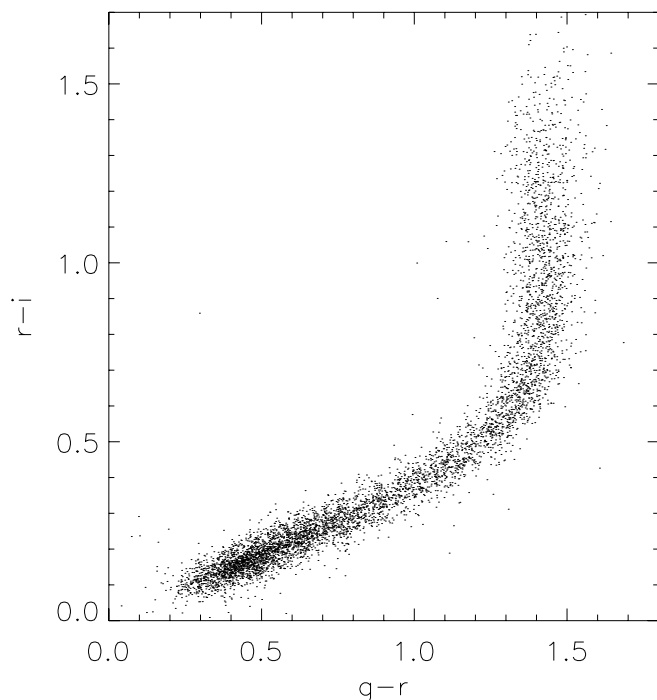
Fig. 8.—A *g-r-i* color-color plot showing the stellar locus, based on the stars in 200 fields from camera column 3 of run 273, restricted to stars with apparent magnitude $r < 19$. The colors are apparent colors based on PSF fluxes with no correction made for Galactic extinction. The IDL code that generated this figure is in § 4.2.
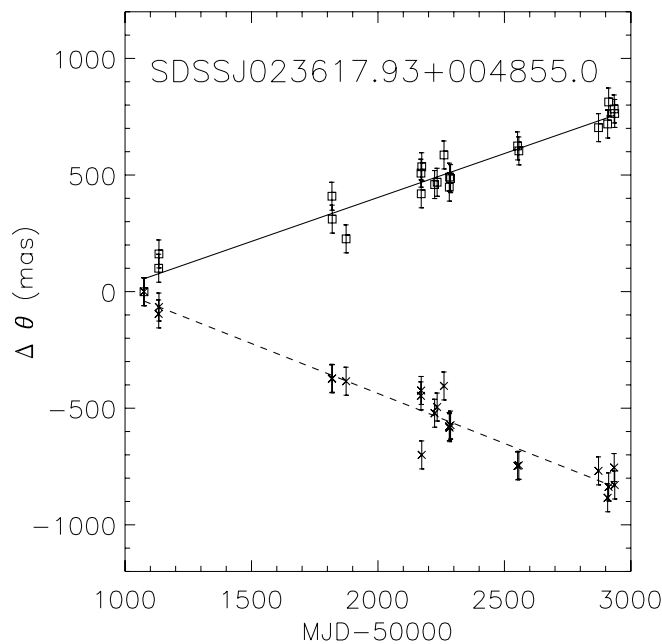

Fig. 9.—Relative position of the L6.5 brown dwarf SDSS J023617.93+ 004855.0 as a function of time. The solid line is a fit to the change in right ascension (relative to its fiducial position; *squares*), while the dashed line is a fit to the change in declination (*crosses*). The errors in the positions are 60 mas in both coordinates. The 22 SDSS observations clearly show the proper motion of this faint object (140 mas yr^{-1} in R.A., -155 mas yr^{-1} in decl.). The code that generated this figure is in § 4.3.

```
; Select the stars -- sdss_selectobj() removes
; stars with these bits set:
;    (BLENDED AND NOT NODEBLEND) OR BRIGHT
; See http://www.sdss.org/dr2/products/catalogs/
;  flags.html for a thorough discussion
indx = sdss_selectobj(objs, objtype='star')
stars = objs[indx]
; Eliminate all saturated stars using flags
; OBJC_FLAGS1, bit 18 -- Saturated
; OBJC_FLAGS2, bit 12 -- Interpolated center
; OBJC_FLAGS2, bit 15 -- PSF flux interpolated

; sdss_flagval() returns 2^(flag bit set)
flag1_template = (sdss_flagval('OBJECT1','SATUR'))
flag2_template = $
  (sdss_flagval('OBJECT2', 'INTERP_CENTER')) + $
  (sdss_flagval('OBJECT2', 'PSF_FLUX_INTERP'))

; Find all objects with none of these flags set
notset = where((((stars.OBJC_FLAGS AND $
                 flag1_template) EQ 0) $
AND ((stars.OBJC_FLAGS2 AND flag2_template) EQ 0))
stars = stars[notset]

; Compute the magnitudes, with a flux floor of
;  1.E-10 nMgy
gmag=22.5 - 2.5*alog10(stars.psfflux[1] > 1.e-10)
rmag=22.5 - 2.5*alog10(stars.psfflux[2] > 1.e-10)
imag=22.5 - 2.5*alog10(stars.psfflux[3] > 1.e-10)

; Pick  stars with r < 19
w = where(rmag LT 19.0)
```

```
; Compute g-r and r-i colors
grcolor = gmag[w] - rmag[w]
ricolor = rmag[w] - imag[w]

; Plot the colors
djs_plot, grcolor, ricolor, ps=3, xr=[0,1.8], $
  yr=[0,1.7], charsize=2, xtitle='g-r', $
  ytitle='r-i', xst=1, yst=1

; Close plot
dfpsclose
```

4.3. *The Proper Motion of a Brown Dwarf*

Multiple observations of the celestial equator enable time-domain studies. A particularly simple example is proper motions; Figure 9 shows the position of nearby L6.5 brown dwarf SDSS J023617.93+004855.0 (Schneider et al. 2002; Geballe et al. 2002) versus time. This object is in the SDSS southern survey equatorial region and has been observed multiple times, both during commissioning observations and during regular survey operations. The right ascension and declination offsets with respect to its fiducial position are shown versus time (MJD). The 22 observations span just over 5 years. The position is taken directly from the pipeline-processed data (for a discussion of SDSS astrometry, see Pier et al. 2003) and clearly show the proper motion of this faint object (140 mas yr^{-1} in right ascension, -155 mas yr^{-1} in declination). The position errors determined from this fit are 60 mas in each coordinate. Several SDSS brown dwarfs were identified in the commissioning and calibration data (Fan et al. 2000), and a project to measure the proper motions of nearby stars and substellar objects is under way.

The following code fragment creates Figure 9; in particular, it demonstrates the use of sdss_findallobj to find multiple observations of objects in the data. Most observations of this object are not yet public; we include them in the figure to show what will be possible with the complete data set.

```
; Open the plot
dfpsplot, 'bd.ps', /color, /square

; This is SDSS J023617.93+004855.0
ra = 39.0747106
dec = 0.8152421

; Find all the observations of this object in
;  rerun 137
imlist = sdss_findallobj(ra, dec, rerun=137)

; Specify the fields to extract
select_tags = ['RUN', 'CAMCOL', 'FIELD', 'ID', $
  'MJD', 'PSFFLUX*', 'RA', 'DEC', 'OFFSET*', $
  'CALIB_STATUS']

; Read in these fields
objs = sdss_readobjlist(inlist=imlist, $
  select_tags=select_tags, /silent)

; Define time axis
dmjd = objs.mjd - 50000

; Compute the change in RA and DEC in mas
dra = (objs.ra - ra)*3.6d6*cos(dec/!radeg)
ddec = (objs.dec - dec)*3.6d6

; Plot the change in RA with time
djs_plot, dmjd, dra, yr=[-1200,1200], yst=1, $
  charsize=2, thick=3, ps=6, xtitle='MJD-50000', $
  ytitle = $'\Delta \theta (mas)'
; Plot typical error of 60 mas
errplot, dmjd, dra-60.0, dra+60.0, thick=3

; Plot the change in DEC with time
djs_oplot, dmjd, ddec, thick=3, ps=7, line=2
; Plot error of 60 mas
errplot, dmjd, ddec-60.0, ddec+60.0, thick=3

; Overplot linear fits
oplot, dmjd, poly(dmjd,linfit(dmjd, dra)), thick=3
oplot, dmjd, poly(dmjd,linfit(dmjd, ddec)), $
  thick=3, line=2

; Output a label
djs_xyouts, 1100, 900, $
  'SDSSJ023617.93+004855.0', charsize=2.5

; Close the plot
dfpsclose
```

4.4. *Star Formation and Young Stellar Objects*

Figure 2 shows a color composite from the three most sensitive SDSS bands (g, r, and i) of a region from runs 259/273 centered on the star-forming region NGC 2068/NGC 2071/HH 24–26. Note the line of Herbig-Haro objects in the outflow jet. Because their emission is dominated by emission lines, Herbig-Haro objects have characteristic colors and can be automatically identified and counted in these regions of high obscuration. We find that there is a very different density distribution of these objects in the Taurus and Orion star-forming regions (Knapp et al. 2004).

The spectral energy distributions of the stars in NGC 2068 and NGC 2071 can be constructed from the five SDSS and three 2MASS bands, giving the luminosity function, the frequency of low-mass objects and the incidence of circumstellar dust. UV-excess objects, that is, young T Tauri stars, can be discovered and mapped across the Orion and Taurus star-forming regions (McGehee et al. 2004b).

4.5. *Structure of the Galactic Halo and Vertical Structure of the Disk*

Because of the depth and color discrimination of SDSS photometry, the SDSS data have enabled major contributions to studies of the structure of the Galactic halo (Yanny et al. 2000; Ivezić et al. 2000; Odenkirchen et al. 2001; Newberg et al. 2003b). These and other studies of distant halo objects (Ibata et al. 1995; Johnston et al. 1995; Majewski et al. 2003; Martínez-Delgado et al. 2004) show the presence of long streams in the halo produced by the tidal disruption of satellite systems (small galaxies and loosely bound globular clusters). The data described herein allow these streams to be traced much closer to the Galactic plane. The SDSS stellar data at low Galactic latitudes can be used to investigate the relationships among the thin disk, the thick disk, and the Galactic halo, tracing the metallicity of each component. The discovery of these halo structures, and the ability of SDSS to follow the structure close to the Galactic plane, provide the impetus for a new initiative, known as SEGUE, to use the SDSS hardware and software to map the structure of the Galactic halo and the disk-halo interface (Newberg et al. 2003a; "Sloan Extension for Galactic Underpinnings and Evolution").

The vast majority of the red stars detected by SDSS are late-type disk dwarfs and subdwarfs. Hawley et al. (2002, 2004) demonstrate a well-established relationship between color and absolute magnitude for dwarfs of spectral type M0 and later, which allows the vertical mapping of the disk to a distance of about 1 kpc from the Galactic plane as well as the three-dimensional distribution of the interstellar dust. Measurements at different Galactic latitudes, especially at low latitudes, allow the measurement of the disk scale length and disk scale height for these stars (McGehee et al. 2004a, 2004b; Jurić et al. 2004).

4.6. *Properties of Interstellar Dust*

Reddening measured by fitting the position of the "blue tip" of the stellar locus in (u, g, r, i, z) color space can be used to investigate possible deviations from the standard extinction law by comparing $E(u-g)$ with $E(g-r)$ in different directions (Finkbeiner et al. 2004). The mosaic images in Figures 2, 3, and 4 demonstrate that the dust clouds also have different emission or reflection properties. In particular, the Taurus dark clouds (Fig. 3) glow at red wavelengths, perhaps because of extended red emission (Witt et al. 1998). Differences between the emission properties of dust clouds, and of the illuminating starlight, can be investigated over large areas with these data.

TABLE A1
calibobj Bookkeeping Values

Name	Type	Description
RUN	LONG	Run number
RERUN	STRING	Rerun name
CAMCOL	LONG	Camera column (1–6)
FIELD	LONG	Field number
ID	LONG	Object ID, starting at 1 and unique in each field
PARENT	LONG	ID of parent, -1 if this is a parent object
NCHILD	LONG	Number of children deblended from this object
MJD	LONG	Modified Julian Day for date of observation
TAI	DOUBLE[5]	Mean time of observation for the object center in each filter, where $TAI = 24 \times 3600 \times MJD$
AIRMASS	FLOAT[5]	Air mass approximated as csc (zenith angle)
PSP_STATUS	LONG[5]	"Status" field from the psField file
CALIB_STATUS...........	INT[5]	Status of photometric calibration

APPENDIX A

STRUCTURE OF THE CALIBOBJ FILES

A current description of the calibObj data format is available at the Web site and is reproduced here in Tables A1–A3 for convenience. Fields unchanged from the fpObjc files are not repeated here and are described in Stoughton et al. (2002).

APPENDIX B

USING INVERSE VARIANCE

Flux errors are expressed as inverse variance ("ivar") in the calibObj files. This is convenient for inverse-variance weighting of combined quantities and handles zero signal-to-noise ratio (ivar = 0) gracefully, as the following example demonstrates.

B1. COLOR CUT

To select all stars with flux ratio r/i greater than some color ratio c with $n\sigma$ confidence, one writes the inequality as $r - ic > n\sigma$, where σ is the uncertainty in the quantity $r - ic$, or

$$\sigma = \left(\frac{1}{I_r} + \frac{c^2}{I_i} \right)^{1/2},$$

TABLE A2
calibobj Calibration Parameters

Name	Type	Description
NMGYPERCOUNT................	FLOAT[5]	Calibration (nanomaggies per count)
NMGYPERCOUNT_IVAR......	FLOAT[5]	Formal error in the photometric calibration as an inverse variance; zero if there were no calibration stars and a default calibration was used instead
CLOUDCAM........................	INT[5]	Photometricity in each filter: -1 = unknown, 0 = cloudy, 1 = clear
EXTINCTION....................	FLOAT[5]	Galactic extinction in magnitudes, defined as $(5.155, 3.793, 2.751, 2.086, 1.479)E(B-V)$, where $E(B-V)$ is from the SFD98 dust maps. Fluxes (and their errors) can be corrected for Galactic extinction as follows: corrected flux = flux $\times 10^{extinction/2.5}$
PIXSCALE........................	FLOAT[5]	Pixel scale (arcsec pixel^{-1})
PSF_FWHM........................	FLOAT[5]	PSF FWHM (arcsec)
PHI_OFFSET....................	FLOAT[5]	Calibration angle (deg) to add to any uncalibrated position angles such that they mean degrees east of north

TABLE A3
calibobj Structure Calibrated Quantities

Name	Type	Description
RA	DOUBLE	J2000 right ascension (deg) in canonical (r-band) filter
DEC	DOUBLE	Declination (deg) in canonical (r-band) filter
OFFSETRA..................	FLOAT[5]	Right ascension of center in this filter relative to RA (arcsec)
OFFSETDEC................	FLOAT[5]	Declination of center in this filter relative to RA (arcsec)
PHI_ISO_DEG.............	FLOAT[5]	Isophotal fit, angle east of north (deg)
PHI_DEV_DEG.............	FLOAT[5]	De Vaucouleurs fit, angle east of north (deg)
PHI_EXP_DEG.............	FLOAT[5]	Exponential fit, angle east of north (deg)
SKYFLUX....................	FLOAT[5]	Sky level (nMgy arcsec^{-2})
SKYFLUX_IVAR...........	FLOAT[5]	
PSFFLUX....................	FLOAT[5]	PSF flux (nMgy)
PSFFLUX_IVAR...........	FLOAT[5]	
FIBERFLUX.................	FLOAT[5]	Fiber flux, 3″ diameter (nMgy)
FIBERFLUX_IVAR	FLOAT[5]	
MODELFLUX.................	FLOAT[5]	Model flux (nMgy)
MODELFLUX_IVAR	FLOAT[5]	
PETROFLUX.................	FLOAT[5]	Petrosian flux (nMgy)
PETROFLUX_IVAR	FLOAT[5]	
DEVFLUX....................	FLOAT[5]	De Vaucouleurs flux (nMgy)
DEVFLUX_IVAR...........	FLOAT[5]	
EXPFLUX....................	FLOAT[5]	Exponential flux (nMgy)
EXPFLUX_IVAR...........	FLOAT[5]	
APERFLUX...................	FLOAT[NAPER,5]	Aperture fluxes (nMgy) in radii of size 0″223, 0″670, 1″024, 1″745, 2″972, 4″584, 7″359, 11″306, 18″020, 27″922, 43″770, 68″307, 106″73, 166″52, and 260″37; our default is to return only those fluxes out to 11″3, unless NAPER is explicitly specified
APERFLUX_IVAR	FLOAT[NAPER,5]	

where I_r and I_i are the r- and i-band inverse variances, respectively. Multiplying by $(I_r I_i)^{1/2}$ yields the inequality

$$(r - ic)\sqrt{I_r I_i} > n\sqrt{I_i + c^2 I_r},$$

which concisely expresses the desired condition without a division by any of the parameters and correctly handles the limiting cases of zero or negative flux, or inverse variance equal to zero (nonmeasurement). The conventional expression of this with magnitudes and σ requires handling the special cases of zero or negative fluxes, or nonmeasurement, in either band.

Many astronomers will want to work with magnitudes, related to nanomaggy fluxes by

$$m = 22.5 - 2.5 \log(\text{flux}),$$

but will find that any flux and color cuts are most easily performed in flux units. These fluxes and magnitudes are on the natural SDSS system and are offset from the true AB system by a few hundredths of a magnitude in each band (see Abazajian et al. 2004 for estimated offsets).

B2. EXTINCTION CORRECTIONS

Extinction values are presented in magnitudes for historical reasons. The extinction estimates provided are based on maps of IR dust emission (Schlegel et al. 1998) and are most reliable in the limit of long wavelengths. Extinction values are given in the calibObj files for each SDSS band, assuming a standard interstellar reddening law of $R_V = 3.1$ in the parameterization of Cardelli et al. (1989). Because the SFD98 dust map is calibrated to $E(B-V)$, it is presented as $E(B-V)$ reddening. This has led to the misunderstanding that the presented $E(B-V)$ is valid for all values of R_V, when in fact it is the near-IR extinction (e.g., SDSS z band) that is roughly constant with changes in R_V. Therefore, if the dust along a given line of sight is known to have a different value of R_V, it is necessary to extrapolate the extinction from a red band (e.g., z band) to the desired band using the appropriate reddening law.

We remind the reader that flux uncertainties must be modified when correcting for extinction. Unlike magnitude uncertainties, which are fractional uncertainties, flux uncertainties are absolute and must be amplified by the same factor as the flux when extinction corrections are applied. To correct flux F and inverse variance I for an extinction of A magnitudes, use

$$F_{\text{corr}} = 10^{0.4A} F, \quad I_{\text{corr}} = 10^{-0.8A} I.$$

REFERENCES

Abazajian, K., et al. 2003, AJ, 126, 2081
———. 2004, AJ, 128, 502
Barth, A. J. 2001, in ASP Conf. Ser. 238, Astronomical Data Analysis Software and Systems X, ed. F. R. Harnden, Jr., F. A. Primini, & H. E. Payne (San Francisco: ASP), 385
Becker, R. H., White, R. L., & Helfand, D. J. 1995, ApJ, 450, 559
Cardelli, J. A., Clayton, G. C., & Mathis, J. S. 1989, ApJ, 345, 245
Cutri, R. M., et al. 2003, Explanatory Supplement to the 2MASS All Sky Data Release (Pasadena: Caltech)

Fan, X., et al. 2000, AJ, 119, 928
Finkbeiner, D. P., et al. 2004, in preparation
Fukugita, M., Ichikawa, T., Gunn, J. E., Doi, M., Shimasaku, K., & Schneider, D. P. 1996, AJ, 111, 1748
Geballe, T. R., et al. 2002, ApJ, 564, 466
Gunn, J. E., et al. 1998, AJ, 116, 3040
Hawley, S. L., et al. 2002, AJ, 123, 3409
———. 2004, in preparation
Høg, E., et al. 2000, A&A, 355, L27 (erratum 363, 385)

Hogg, D. W., Finkbeiner, D. P., Schlegel, D. J., & Gunn, J. E. 2001, AJ, 122, 2129

Ibata, R. A., Gilmore, G., & Irwin, M. J. 1995, MNRAS, 277, 781

Ivezić, Ž., et al. 2000, AJ, 120, 963

Johnston, K. V., Spergel, D. N., & Hernquist, L. 1995, ApJ, 451, 598

Jurić, M., et al. 2004, in preparation

Knapp, G. R., et al. 2004, in preparation

Kniazev, A. Yu., Grebel, E. K., Hao, L., Strauss, M. A., Brinkmann, J., & Fukugita, M. 2003, ApJ, 593, L73

Lupton, R. H., Gunn, J. E., Ivezić, Ž., Knapp, G. R., Kent, S., & Yasuda, N. 2001, in ASP Conf. Ser. 238, Astronomical Data Analysis Software and Systems X, ed. F. R. Harnden, Jr., F. A. Primini, & H. E. Payne (San Francisco: ASP), 269

Lupton, R. H., Gunn, J. E., & Szalay, A. S. 1999, AJ, 118, 1406

Lupton, R. H., Ivezić, Ž., Gunn, J. E., Knapp, G., Strauss, M. A., & Yasuda, N. 2002, Proc. SPIE, 4836, 350

Lupton, R. H., et al. 2004, in preparation

Majewski, S., Skrutskie, M. F., Weinberg, M. D., & Ostheimer, J. C. 2003, ApJ, 599, 1082

Martínez-Delgado, D., Gómez-Flechoso, M. A., Aparacio, A., & Carrera, R. 2004, ApJ, 601, 242

McGehee, P. M., Anderson, K. S. J., Hobbs, L. M., & York, D. G. 2004a, in preparation

McGehee, P. M., et al. 2004b, in preparation

Monet, D.G., et al. 2003, AJ, 125, 984

Newberg, H. J., et al. 2003a, BAAS, 203, No. 112.11

———. 2003b, ApJ, 596, L191

Odenkirchen, M., et al. 2001, ApJ, 548, L165

Oke, J. B., & Gunn, J. E. 1983, ApJ, 266, 713

Pier, J. R., Munn, J. A., Hindsley, R. B., Hennessy, G. S., Kent, S. M., Lupton, R. H., & Ivezić, Ž. 2003, AJ, 125, 1559

Schlegel, D. J., Finkbeiner, D. P., & Davis, M. 1998, ApJ, 500, 525 (SFD98)

Schlegel, D. J., et al. 2004, in preparation

Schneider, D. P., et al. 2002, AJ, 123, 458

Smith, J. A., et al. 2002, AJ, 123, 2121

Stoughton, C., et al. 2002, AJ, 123, 485

Witt, A. N., Gordon, K. D., & Furton, D. G. 1998, ApJ, 501, L111

Yanny, B., et al. 2000, ApJ, 540, 825

York, D. G., et al. 2000, AJ, 120, 1579

Zacharias, N., Rafferty, T. J., & Zacharias, M. I. 2000, in ASP Conf. Ser. 216, Astronomical Data Analysis Software and Systems IX, ed. N. Manset, C. Veillet, & D. Crabtree (San Francisco: ASP), 427